1 # Modelling and parameter estimation of diethyl phthalate partitioning

2 # behaviour on glass and aluminum surfaces

3

4 Simoní Da Ros[†]*, Katherine Curran[†]*

5 [†] UCL Institute for Sustainable Heritage, University College London, 14 Upper Woburn

6 Place, London WC1H 0NN, United Kingdom.

7 *Correspondence authors: s.ros@ucl.ac.uk (Simoní Da Ros), k.curran@ucl.ac.uk (Katherine

8 Curran).

9 *Abstract:* The knowledge of the partitioning behaviour of semi-volatile organic compounds

10 (SVOCs), such as phthalates, between different materials and their surrounding air is of

11 extreme importance for quantifying levels of human exposure to these compounds, which have

12 been associated with adverse health effects. Phthalates' partitioning behaviour also represents

13 a key property for modelling and assessing polymer degradation mechanisms associated with

14 plasticiser loss. However, the characterisation of phthalates partitioning behaviour has been

15 reported only for a limited number of compounds, mainly involving di-2-ethylhexyl phthalate

16 (DEHP), di-isononyl phthalate (DINP) and di-isodecyl phtahalate (DIDP), while the

17 characterisation of diethyl phthalate (DEP) partitioning has been overlooked. As one of the

18 first plasticisers employed in the production of semi-synthetic plastics produced industrially in

19 the late 19th and early 20th century, DEP plays an important role for understanding stability

20 issues associated with historically significant artefacts in museum collections and archives.

21 Here we show that the partitioning behaviour of DEP between borosilicate glass and aluminum

22 surfaces and their surrounding air can be described by an exponential function of temperature,

23 presenting a model to describe this relationship for the first time. Model parameters are

24 estimated using nonlinear regression from experimental measurements acquired using 109

25 samples which have been equilibrated at different temperatures between 20 and 80 ˚C in sealed

26 environments. Measured partition coefficients have been predicted accurately by our proposed

27 model. The knowledge of DEP equilibrium distribution between adsorptive surfaces and

28 neighbouring environments will be relevant for developing improved mathematical

29 descriptions of degradation mechanisms related to plasticiser loss.

32

1. Introduction

Semi-volatile organic compounds (SVOCs), such as phthalates, can partition between different materials and their surrounding air in indoor environments, affecting levels of human exposure to these compounds, which have been associated with adverse health effects, including endocrine disruption, cancer, birth defects and alteration of insulin signalling molecules which could trigger type 2 diabetes (Miles-Richardson, 2017; Mondal and Mukherjee, 2020). Thus, understanding the distribution of these compounds is fundamental for properly assessing and quantifying levels of human exposure (Cao et al., 2016; Eichler et al., 2018; Xu and Little, 2006). Characterising the partitioning behaviour of phthalates is also of extreme importance to allow for the mathematical description of material degradation processes, including, for instance, degradation mechanisms in plastic objects which can be initiated or promoted by the loss of phthalates plasticisers (King et al., 2020).

Diethyl phthalate (DEP) represents one of the first plasticisers employed industrially in the production of semi-synthetic plastics in the late 19th and early 20th century (Macht and Fletcher, 1938; Mossman, 1997; Walsh et al., 1933; Zimmerli, 1932). Therefore, understanding diethyl phthalate loss is important for addressing stability issues associated with historically significant artefacts in museum collections and archives. For instance, the loss of plasticisers such as DEP from cellulose acetate-based artefacts is known to initiate or promote physical changes, such as warping, crazing, cracking and brittleness, which could ultimately reduce the value of these art objects (Da Ros et al., 2021; Richardson et al., 2014; Shashoua, 2008; Strlič et al., 2013). Furthermore, although the partial substitution of DEP by less volatile phthalates has led to a reduction of its worldwide consumption (IHS Markit, 2018), DEP still finds application in a wide range of consumer products, including orthodontic adhesives and dentures, cosmetic formulations (such as bath oils, tablets and salts; eye shadow, perfumes, hair sprays, nail polish and enamel removers, nail extenders, detergents, aftershave lotions and

58 skin care products), and pharmaceutical products (such as in coatings for drug controlled

59 release) (Mondal and Mukherjee, 2020; Sekizawa et al., 2003; Wypych, 2017).

60 Thus, it is not surprising that DEP is still found as an important constituent of pollutants

61 in indoor (Fromme et al., 2004; Yang et al., 2020) and outdoor (Vasiljevic et al., 2021)

62 environments. However, while research has advanced on understanding the partition behaviour

63 of phthalates such as di-2-ethylhexyl phthalate (DEHP), benzyl butyl phthalate (BBP), di-n-

64 butyl phthalate (DnBP) and di-isobutyl phthalate (DiBP) on a wide range of materials (Wei et

65 al., 2018), our knowledge on the partition behaviour of DEP remains limited to a few systems,

66 Table 1. For instance, the partition coefficient of DEP between cotton fabric and air, $K_{cotton-air}$,

67 has been reported as equal to $2.6 \cdot 10^5$ (unitless) at 25 ˚C by a study which highlighted the risks

68 of non-dietary phthalate ingestion by toddlers mouthing cotton and dermal uptake (Morrison

69 et al., 2015a). In another study, the relationship between temperature and $K_{cotton-air}$ values for

70 DEP between 20 and 40 ˚C was reported, where an approximately exponential reduction in

71 $K_{cotton-air}$ with the increase of temperature was demonstrated (Eftekhari and Morrison, 2018),

72 corroborating similar observations reported for additional phthalates between vinyl flooring

73 and air (Bi et al., 2015).

74

75 **Table 1** - Partition coefficients calculated or experimentally measured for diethyl phthalate

76 for different systems.

Based on the ratio between	K (unitless)	T (˚C)	Ref.
Indoor airborne particles/air	$1.8 \cdot 10^{-4}$ [a] $0.67 \cdot 10^{-4}$ [b]	25	(Weschler et al., 2008)
Octanol/air	$3.5481 \cdot 10^7$	25	(Cousins and Mackay, 2000)[c]
Air/water Octanol/water	$9.7724 \cdot 10^{-6}$ 346.7	25	(Cousins and Mackay, 2000)[c]
Octanol/water	263.03	25	(Ellington and Floyd, 1996)

Polydimethylsiloxane/water	59 ± 14		
Polydimethylsiloxane/water	53.70		
Polyacrylate/water	218 ± 10	22	(Kotowska et al., 2006)
Hexane/acetonitrile	0.09 ± 0.01		
Hexane/nitromethane	0.07 ± 0.01		
Outershirt cotton fabric/air	$2.6 \cdot 10^5$		
Undershirt cotton fabric/air	$2.5 \cdot 10^5$	25	(Morrison et al., 2015a)
Jeans cotton fabric/air	$2.7 \cdot 10^5$		
Jeans cotton fabric/air	$(5.6 \pm 0.2) \cdot 10^5$	20	(Eftekhari and Morrison, 2018)
	$(1.5 \pm 0.01) \cdot 10^5$	25	
	$(1.1 \pm 0.1) \cdot 10^5$	32	
	$(0.75 \pm 0.01) \cdot 10^5$	40	
Cotton fabric/air	630957	20-35	(Saini et al., 2017)
Rayon fabric/air	1584893		
Latex wall paint/air	$1.6596 \cdot 10^7$	23.8	(Schripp et al., 2014)
	$2.0417 \cdot 10^7$	23.3	
	$3.5481 \cdot 10^7$	23	
	$2.7542 \cdot 10^7$	30	
	$2.3442 \cdot 10^7$	28.6	
PVC film (5 wt%)/n-hexane	521.87	20	
	10.02	40	
	10.39	60	
PVC film (5 wt%)/isooctane	5233.33	20	(Yuan et al., 2019)
	513.80	40	
	30.71	60	
PVC film (5 wt%)/ethanol	1057.53	20	
	131.04	40	
	6.77	60	

77   [a]Calculated using correlation developed by (Naumova et al., 2003) for polycyclic aromatic hydrocarbons;

78   [b]Calculated using correlation developed by (Finizio et al., 1997) using octanol/air partition coefficients for

79 polyclic aromatic hydrocarbons; [c]Calculated using correlations developed using water and air solubility and

80 octanol/water partition coefficients for phthalate esters.

81

82 As it can be seen from Table 1, there are many indoor built materials for which the

83 partition behaviour of DEP is unknown, including impervious surfaces such as glass and

84 aluminum. However, due to their presence in a variety of domestic interior surfaces, in addition

85 to many scientific laboratory tools and instruments, characterising the partitioning of DEP on

86 these surfaces is essential for understanding how DEP is transported and distributed through

87 environments. For instance, environmental chambers used in emission studies are usually made

88 of glass and/or aluminum elements (Afshari et al., 2003; Clausen et al., 2004; Even et al., 2020;

89 Xu and Little, 2006), and glass and/or aluminum are also often involved in experimental

90 methods concerning measurements of phthalates concentrations (Clausen et al., 2016;

91 Eftekhari and Morrison, 2018; Vasiljevic et al., 2021).

92 In this context, the partitioning of DEHP on aluminum, steel, glass and acrylic surfaces

93 has been characterised at 25 ˚C (Wu et al., 2017), suggesting that $K_{i\text{-}air}$ values for DEHP could

94 depend not only on the nature of the adsorptive surface, but also on its roughness, defined as

95 the ratio between the true surface area and the geometric area of the material. In another study,

96 the characterisation of the partitioning of triethyl phosphate (TEP), tributyl phosphate (TBP)

97 and tris-(chloropropyl)-phosphate (TCPP) on borosilicate glass has also indicated the likely

98 existence of a relationship between these compounds' volatility and their partition coefficients

99 at 23 ˚C (Ghislain et al., 2017), a finding also observed for the partitioning behaviour of DINP,

100 DEHP, BBP and DnBP over stainless steel at 25 ˚C (Liang and Xu, 2014a).

101 However, even for the most widely researched SVOCs, significantly different partition

102 coefficients have been reported at similar temperatures, stressing the urgent need for further

103 research in this field, as also pointed out by (Wei et al., 2019). For instance, values for the

partition coefficient of DEHP on glass surfaces have been reported as equal to 3800 m at 22 ˚C (Xu and Little, 2006), 600 m at 25 ˚C (Wu et al., 2017) and 0.26 m at 23 ˚C (Ghislain et al., 2017).

Thus, this work has characterised the partitioning behaviour of DEP on glass and aluminum surfaces for the first time in a wide range of temperatures ranging between 20 and 80 ˚C. Additionally, we quantified the effect of temperature on the partitioning behaviour of DEP between these surfaces and their surrounding air, presenting a model to describe this relationship. Model parameters are estimated using nonlinear regression from experimental measurements acquired using 109 samples which have been equilibrated between 20 and 80 ˚C in sealed environments. The knowledge of DEP equilibrium distribution between adsorptive surfaces and neighbouring environments will be relevant for developing improved mathematical descriptions of degradation mechanisms related to plasticiser loss. Furthermore, we anticipate our model to be a starting point for understanding and quantifying the partition behaviour of DEP in additional systems.

2. Materials and Methods

2.1 Determination of DEP partitioning between enclosure surfaces and air

Sample enclosures used in this work consisted of 20 mL borosilicate glass vials (referred to here as "enclosure vials") equipped with a polypropylene lid presenting a pulp-backed aluminum foil liner inner surface, which were acquired from Fisher Scientific (London, catalogue number 12383317). Vials were dried at 150 ˚C (glass) and 90 ˚C (lid) for 12 h prior to experiments to minimise contamination. In order to measure the equilibrium concentration ratio of DEP between the inner surfaces of the enclosure vial and the gas-phase within, a smaller, open 2 mL glass vial, filled with 1 mL of pure DEP (99.5 %, purchased from Sigma Aldrich, London, used as received), was placed at the centre of the enclosure vial, as illustrated

129   in Fig. S1. After the enclosure vial was sealed, the system was then equilibrated at different

130   temperatures (20, 30, 40, 50, 60, 70, 80 and 90 ˚C) by keeping the vials in environments with

131   temperature control. The actual temperature and relative humidity (RH) during the

132   experimental period were recorded using TinyTag dataloggers. Several replicated experiments

133   at each temperature were performed to guarantee reproducibility and assess equilibration,

134   totalling 109 individual measurements.

135   At the end of the experiment, enclosure vials were removed from ovens and allowed to

136   stabilise at room temperature while still sealed for approximately 1 h to minimise fluctuations

137   that would otherwise be present were vials analysed while still hot. DEP-containing vials were

138   then removed using tweezers and the aluminum and glass vial inner surfaces were immediately

139   and individually washed with 4 mL of solvent each. Finally, washing solutions were analysed

140   by UV-Vis spectroscopy, as detailed in the next section.

141   *2.2 Quantification of DEP adsorbed on enclosure surfaces*

142   The UV-Vis spectroscopic method used to quantify the amount of DEP adsorbed on

143   the sample enclosure surface was based on the absorbance intensity of DEP at 226 nm

144   (Monakhova et al., 2011). Calibration solutions were prepared by diluting a stock solution of

145   DEP, prepared at the concentration of 15 mg·mL^{-1}, using an aqueous ethanolic solution (60/40

146   %vol. ethanol/distilled water) as solvent. Ethanol (96 %vol.) was purchased from Fisher

147   Scientific (London, UK) and used without further purification. Measurements were performed

148   in a double-beam Shimadzu spectrophotometer 2700 using quartz cuvettes of 1 cm pathlength.

149   After each analysis, the quartz cuvette was washed and the solvent analysed for phthalate

150   contamination. This procedure was performed also to ensure that the quartz cuvette was free

151   from contamination from the preceding analysis. Spectra were recorded between 200 and 350

152   nm with a spectral resolution of 1 nm, as illustrated in the Fig. S2 of the Supplementary

153   Information (*SI*). A seven-point calibration curve ranging between 0.47 and 18.75 µg·mL^{-1}

154 DEP was always built at the beginning of the analysis day, as illustrated in Fig. S3 of the *SI*.

155 Limits of quantification (LOQ) ranged between 22.6 and 58.6 ng among calibrations and were

156 well below quantified ranges among experiments.

157   The efficiency of the washing procedure applied for transferring the DEP from the

158 sample enclosure surface to the solvent solution prior to UV-Vis spectroscopic measurements

159 was evaluated by four replicated experiments in which an accurate amount of DEP (5.60, 0.86,

160 0.79 and 0.76 mg) was added within a sample enclosure vial that was then sealed and allowed

161 to stabilise at 60 ˚C for 13 h. Washing solutions were diluted accordingly to result in

162 absorbances within the linear range of the calibration curve. From these, an average recovery

163 efficiency of 105.95 ± 7.01 % was recorded, as further illustrated in Table S1 of the SI, which

164 was considered excellent (Cao et al., 2016; Ghislain et al., 2017; Wu et al., 2017).

165

166 *2.3 Modelling the effect of temperature on DEP partitioning between enclosure surfaces and*

167 *air*

168   The partition coefficient of DEP, $K_{i\text{-}air}$, between the sample enclosure surface i (where

169 i represents either the glass or aluminum vial inner surface) and the DEP gas-phase

170 concentration, $C_{g,DEP}$, was calculated using Eq. (1), in which $C_{s,i}$ represents the quantified

171 amount of DEP adsorbed on the surface i, in mg·m^{-2}.

172     $K_{i-air} = \dfrac{C_{s,i}}{C_{g,DEP}}$ (1)

173   Values of $C_{g,DEP}$, in mg·m^{-3}, at each experimental temperature, T (in Kelvin), were

174 calculated using Eq. (2), in which the DEP saturation vapour pressure, p^*, was calculated using

175 the three-parameter form of the Cox equation, Eq. (3) (Roháč et al., 2004). In Eq. (2), M_{DEP} is

176 the molecular mass of DEP and R is the ideal gas constant. In Eq. (3), p_0 and T_0 represent the

177 pressure and temperature at the triple-point, equal to 0.0029 Pa and 269.922 K, respectively,

178   and A_0, A_1 and A_2 denote the coefficients estimated by (Roháč et al., 2004), equal to 3.844479,

179   -9.201487·10^{-4} and -5.406641·10^{-7}, respectively.

180
$$C_{g,DEP} = \left(\frac{p^*}{RT} \cdot M_{DEP} \right) \times 1000 \tag{2}$$

181
$$\ln\left(\frac{p^*}{p_0} \right) = \left(1 - \frac{T_0}{T} \right) \exp(A_0 + A_1 \cdot T + A_2 \cdot T^2) \tag{3}$$

182   In order to calculate $C_{s,i}$ in mg·m^{-2}, the quantified amount of DEP adsorbed on the

183   sample enclosure surface, in mg, was divided by the geometric exposed area, A, which was

184   calculated as equal to 43.99 and 2.01 cm^2 for the glass and aluminum surfaces, respectively,

185   from the vial dimensions, Fig. S1.

186   Finally, the dependence of obtained $K_{i\text{-}air}$ values towards temperature was quantified

187   using a reparameterised form of the van't Hoff equation, Eq. (4), to minimise the correlation

188   of estimated coefficients (Koretsky, 2013; Schwaab and Pinto, 2007a). In Eq. (4), T is the

189   measured temperature, in K, and T_{ref} was defined as equal to 322 K for both the glass and

190   aluminum surfaces. Usually, T_{ref} is defined as the average temperature of the analysed

191   experimental range, even though the choice criterion for T_{ref} should be based on its capacity to

192   reduce or minimise the correlation between parameters estimates (Schwaab and Pinto, 2007a).

193   Thus, we performed several parameter estimation procedures using different T_{ref} values within

194   the experimental range to assess its impact on resultant estimated coefficients correlation,

195   resulting in the selection of 322 K as T_{ref}.

196
$$K_{i-air} = \exp\left(A_i + B_i \left(\frac{T - T_{ref}}{T} \right) \right) \tag{4}$$

197 In Eq. (4), the A_i constant is related to the pre-exponential factor of the integrated form of the

198 van't Hoff equation, $K_{i-air,T_{ref}}$, according to Eq. (5) and B_i relates to the DEP

199 adsorption/desorption enthalpy, $\Delta H°$, according to Eq. (6).

200 $A_i = \ln(K_{i-air,T_{ref}})$ (5)

201 $B_i = \dfrac{\Delta H°}{R \cdot T_{ref}}$ (6)

202 Thus, a constant enthalpy for the DEP adsorption/desorption was assumed, which was

203 considered a reasonable hypothesis given that all experiments were performed at atmospheric

204 pressure and low temperatures.

205

206 *2.4 Parameter estimation and statistical evaluation of results*

207 The estimation of the A_i and B_i parameters from Eq. (4) was performed through the

208 minimisation of the weighed-least-squares objective function (Da Ros et al., 2017b; Schwaab

209 and Pinto, 2007b), $F_{obj}(\theta)$, Eq. (7), in which NE is the number of experimental data points, K_{i-}

210 $_{air,j}{}^{exp}$ denotes the experimental value at the experimental conditions j as calculated from

211 UV-Vis spectroscopic measurements, $K_{i-air,j}{}^{mod}$ is the value predicted using Eq. (4), $x_j{}^{exp}$

212 represents the experimental condition of temperature, θ represents a vector with the best set of

213 parameter estimates for A_i and B_i, and $\sigma_j{}^2$ denotes the variance associated with the measurement

214 fluctuations of $K_{i-air,j}{}^{exp}$ at the experiment condition j.

215 $F_{obj}(\theta) = \sum_{j=1}^{NE} \dfrac{\left(K_{i-air,j}^{exp} - K_{i-air,j}^{mod}(x_j^{exp}, \theta)\right)^2}{\sigma_j^2}$ (7)

216 The minimisation of Eq. (7) was performed using a hybrid optimisation method

217 implemented in Fortran 90, in which the Particle Swarm Optimization (PSO) algorithm

218 (Kennedy, J., Eberhart, 1995) is used in the initial phase of minimisation (Noronha et al., 1993;

219   Schwaab et al., 2008). The best estimate of the point of the minimum is used as an initial guess

220   for a second estimation round, using the Gauss-Newton method (Da Ros et al., 2017b; Schwaab

221   and Pinto, 2007b). The initial phase of minimisation using the PSO algorithm was performed

222   using 30 particles and 50000 iterations, resulting in 1500000 evaluations of the objective

223   function. Convergence was achieved when the relative modification of the objective function

224   was smaller than 1.0×10^{-6}. Statistical significance of parameters estimates was assessed with

225   the standard t-test (Box, G.P., Hunter, J.S., Hunter, 2005), with 95 % confidence level. The

226   quality of the A_i and B_i parameter estimates was further assessed by evaluating the parameters

227   correlation according to Eq. (8), in which v_{ij} represents the element ij of the covariance matrix

228   of parameter estimates, $V_{\boldsymbol{\theta}}$, defined by Eq. (9), where $\boldsymbol{B}$ is the sensitivity matrix that contains

229   the first derivatives of the model responses in respect to the model parameters and V_y denotes

230   the covariance matrix of experimental fluctuations (Schwaab et al., 2008).

231    $$\rho_{ij} = \frac{v_{ij}^2}{\sqrt{v_{ii}^2 v_{jj}^2}} \tag{8}$$

232    $$V_{\boldsymbol{\theta}} = \left[\boldsymbol{B}^T V_y \boldsymbol{B} \right]^{-1} \tag{9}$$

233   Additionally, the likelihood confidence region of A_i and B_i parameter estimates was

234   characterised by Eq. (10) (Beale, 1960; Schwaab et al., 2008), where $F_{obj}(\hat{\theta})$ represents the

235   objective function at the point of minimum, NP is the number of parameters, and $F_{NP,NE-NP}^{\alpha}$ is

236   the F probability distribution value for NP and $NE-NP$ degrees of freedom and 95 % confidence

237   level, which is equal to 6.94 in this work.

238    $$F_{obj}(\theta) \leq F_{obj}(\hat{\theta})\left(1 + \frac{NP}{NE-NP} F_{NP,NE-NP}^{\alpha}\right) \tag{10}$$

239   Finally, the evaluation of the model adequacy was performed by comparing the final value of

240   the objective function (*Final SSE*) with the limits of the *Chi-square* distribution with *NE-2*

241   degrees of freedom and 95 % confidence level (Schwaab and Pinto, 2007b). In addition, model

242   predictions were compared with experimental measurements, in which prediction errors were

243   calculated by Eq. (11).

244   $\widehat{V}_y = BV_\theta B^T$ (11)

245   **3. Results and Discussion**

246   *3.1 Assessment of equilibrium*

247   To verify that equilibration had occurred in each investigated condition, a period of at

248   least 4-52 days was selected for our experiments. Fig. 1 illustrates the quantified amounts of

249   DEP adsorbed on the inner glass surface of the enclosure vials, m_{glass}, as a function of time. As

250   it can be seen, measurements supported the hypothesis that equilibration times were long

251   enough to allow the system to equilibrate at each temperature. A similar conclusion could be

252   inferred from measurements on the aluminum surface of the enclosure vials, Fig. S4.

253   It is important to note that observed equilibration times are in agreement with previous

254   findings. For instance, the adsorption of DEHP, emitted from a PVC flooring containing 23 ±

255   3 wt % of DEHP, on aluminum, polished glass and acrylic surfaces was estimated to equilibrate

256   after 13 h at 25 ˚C in an approximately 0.45 cm^3 sealed chamber presenting an emitting source

257   and adsorptive surface area of 3.2 cm^2 (Wu et al., 2017). In
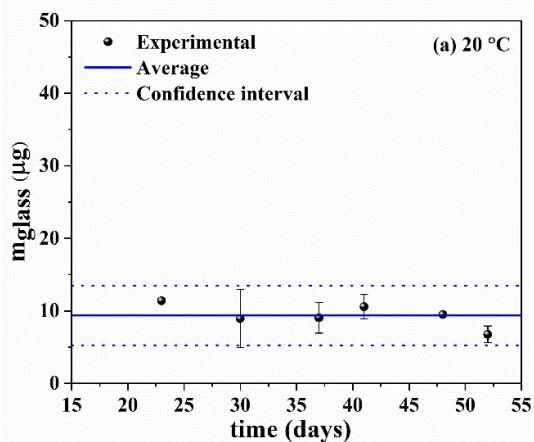
258
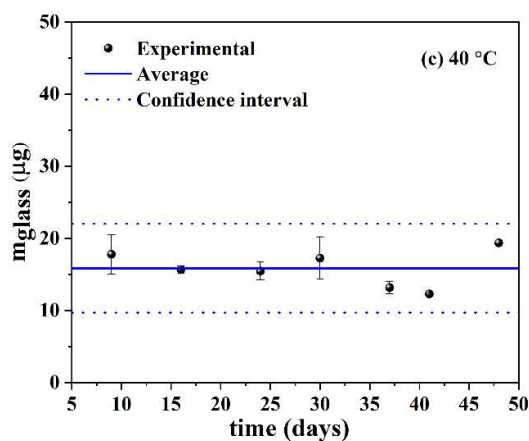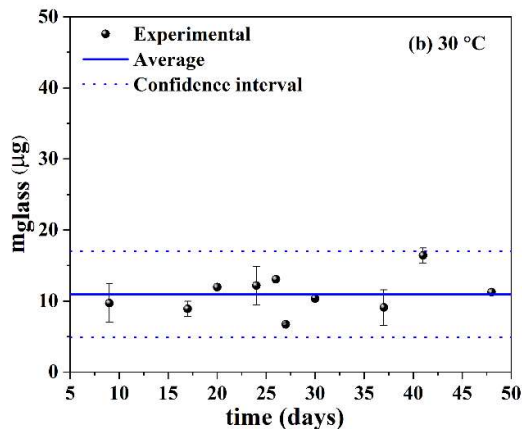
259
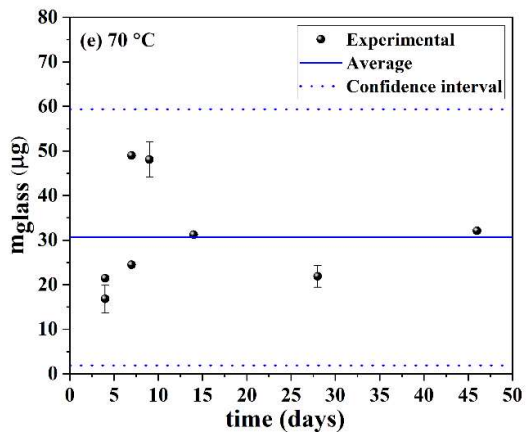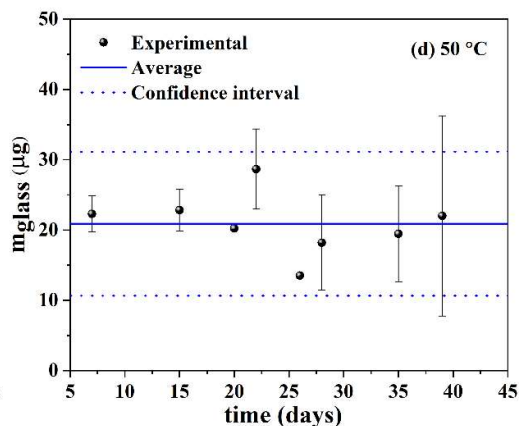
260
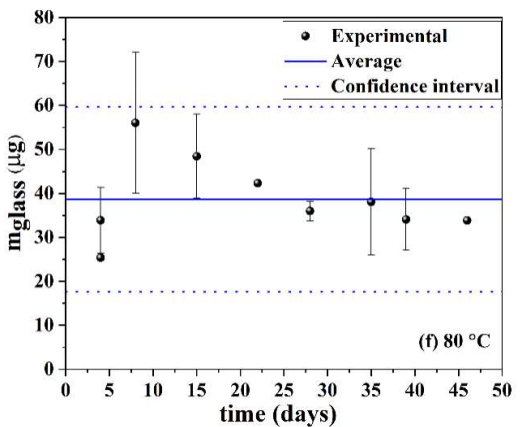
261 **Fig. 1** - Quantified DEP on the vial inner glass surface (in μg), m_{glass}, as a function of

262 equilibration time at 20, 30, 40, 50, 70 and 80 ˚C. Equilibration data at 60 ˚C is presented as

263 Fig. S5. Error bars represent absolute standard deviations (σ). The confidence interval (--) was

264 built assuming averages ($\bar{u}$, —) follow the *t-Student* distribution of probabilities with *NE-1*

14

265   degrees of freedom and 95% confidence level, where *NE* denotes the total number of

266   measurements (●) at each temperature, as $\bar{u} \pm \sigma \times$ *t-Student*.

267   another example, the adsorption TEP, TBP and TCPP emitted from a polyurethane foam

268   containing between 5 and 7.6 wt% of the above compounds, on borosilicate glass was observed

269   to equilibrate after between 2 to 5 h at 23 ˚C in a 60 cm^3 sealed chamber presenting an emitting

270   source of 17 cm^2 and an adsorptive surface of approximately 50 cm^2 (Ghislain et al., 2017).

271   Therefore, it follows that the adsorption equilibration time of diethyl phthalate, a more

272   volatile compound when compared to DEHP, TBP and TCPP, involving its diffusion from the

273   layer just above its pure liquid state to the surrounding air and adsorptive surfaces within the

274   sealed sample enclosures used in this work, was expected to be shorter than the above-

275   mentioned examples, further supporting our conclusion that acquired measurements had

276   achieved equilibration.

277   *3.2 Modelling the effect of temperature on the DEP partitioning between enclosure surfaces*

278   *and air*

279   Fig. 2 illustrates the relationship between adsorbed quantities and temperature for the

280   glass and aluminum surfaces. This figure presents the global averages of adsorbed DEP, as

281   illustrated in Fig. 1 and S4 ($\bar{u}$, —), divided by the respective geometrical area of the exposed

282   surface, resulting in global averages of DEP concentrations on the glass, $C_{s,glass}$, and aluminum,

283      $C_{s,Al}$, surfaces, in mg·m^{-2}.

284   As it can be seen from Fig. 2, while an exponential increase in $C_{s,glass}$ was observed as

285   the equilibration temperature was raised, the same tendency was not verified for $C_{s,Al}$. This

286   could indicate that experimental fluctuations associated with measurements on the aluminum

287   surface were too large to allow for the observation of the temperature effect. Indeed, while

288   adsorbed DEP quantities ranged between approximately 9.4 and 38.7 µg for the glass surface

289   among investigated temperatures, this amount for the aluminum surface was significatively
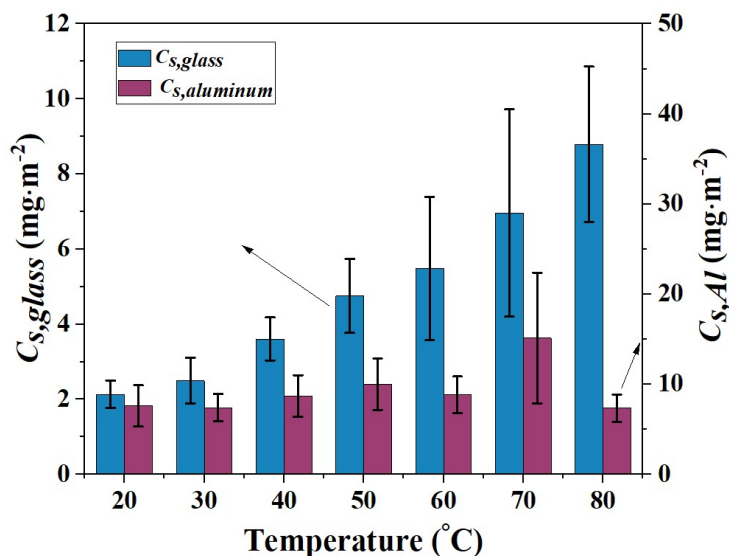
290

291   **Fig. 2 -** Quantified DEP concentration averages obtained for the borosilicate glass, $C_{s,glass}$, and

292   aluminum, $C_{s,Al}$, surfaces from replicated experiments as a function of equilibration

293   temperature. Error bars represent absolute standard deviations.

294

295   smaller, ranging between 1.5 and 3 µg (but still well above LOQ). In general, this resulted in

296   more precise measurements associated with the glass surface, which presented global relative

297   standard deviations (RSDs) ranging from 15.9 to 39.6 %, being smaller than 24 % for 5 of the

298   7 experimental conditions investigated. For the aluminum surface, RSDs values varied between

299   20 and 48 %, being smaller than 28 % for 5 of the 7 experimental conditions.

300   Regardless of the distinct variabilities among experimental conditions, indicating, as

301   expected, that the precision of measurements could depend on the range of concentrations

302   analysed (Da Ros et al., 2017a), one must note that several replicates have been performed to

303   ensure the reproducibility of experimental measurements, as already illustrated in Fig. 1 and

304   S4. Thus, global averages obtained for $C_{s,glass}$ and $C_{s,Al}$ were considered suitable for calculating

305   DEP partition coefficients between the adsorptive surfaces and the surrounding gas-phase,

306 $K_{glass\text{-}air}$ and $K_{Al\text{-}air}$, calculated using Eqs. (1-3), and resultant values are summarised in Table

307 2, along with average temperatures, relative humidities (RH) and DEP surface concentrations

308 quantified at each equilibration condition.

309

310 **Table 2** – Average temperature, relative humidity (RH), DEP surface concentrations and

311 partition coefficients quantified at each equilibration condition along with respective absolute

312 standard deviations.

T (˚C)	RH (%)	$C_{s,glass}$ (mg·m^{-2})	$C_{s,Al}$ (mg·m^{-2})	$K_{glass\text{-}air}$ (m)	$K_{Al\text{-}air}$ (m)
20.1 ± 0.18	51 ± 6.4	2.13 ± 0.36	7.60 ± 2.3	4.11·10^{-1} ± 6.97·10^{-2}	1.47 ± 4.43·10^{-1}
32.2 ± 0.56	17 ± 2.1	2.49 ± 0.61	7.41 ± 1.5	1.41·10^{-1} ± 3.43·10^{-2}	4.18·10^{-1} ± 8.46·10^{-2}
39.1 ± 0.12	16.4 ± 2.4	3.61 ± 0.57	8.7 ± 2.31	9.72·10^{-2} ± 1.54·10^{-2}	2.34·10^{-1} ± 6.23·10^{-2}
50.0 ± 0.03	8.6 ± 1.7	4.75 ± 0.99	10 ± 2.86	4.73·10^{-2} ± 9.81·10^{-3}	9.96·10^{-2} ± 2.85·10^{-2}
59.9 ± 0.03	6.1 ± 0.7	5.48 ± 1.91	8.82 ± 2.04	2.45·10^{-2} ± 8.54·10^{-3}	3.95·10^{-2} ± 9.11·10^{-3}
70.1 ± 0.05	5.9 ± 0.5	6.97 ± 2.76	15.13 ± 7.27	1.32·10^{-2} ± 5.24·10^{-3}	2.87·10^{-2} ± 1.38·10^{-2}
79.3 ± 0.04	4.9 ± 0.3	8.79 ± 2.07	7.33 ± 1.52	8.48·10^{-3} ± 2.0·10^{-3}	7.07·10^{-3} ± 1.46·10^{-3}

313

314 Furthermore, one should also note that as values of DEP partial pressure rise with

315 temperature, increasing the DEP gas-phase concentration, $C_{g,DEP}$, Eqs. (2-3), the observed

316 reduction in $K_{glass\text{-}air}$ and $K_{Al\text{-}air}$ values with temperature could be expected. However, as

317 calculated $K_{glass\text{-}air}$ and $K_{Al\text{-}air}$ values represent independent measurements at each temperature

318 which also take into account the adsorptive properties of the investigated surfaces (Eq. (1)),

319 quantified values of $K_{glass\text{-}air}$ and $K_{Al\text{-}air}$ can be used to assess the relationship between these

320 partition coefficients and temperature, through Eqs. (4-6).

321 In order to model the effect of temperature, values of temperature (in Kelvin) and $K_{i\text{-}air}$

322 as presented in Table 1 were used to adjust Eq. (4), as described in Sections 2.3 and 2.4.

323 However, measurements obtained at 40 ˚C were not included in the parameter estimation, to

324 allow them to be used as an independent validation set. Fig. 3 illustrates the $K_{i\text{-}air}$ predicted and

325 experimental values for the borosilicate glass (a) and aluminum (b) surfaces; estimated

326 parameters of Eq. (4) are summarised in Table 3.

327
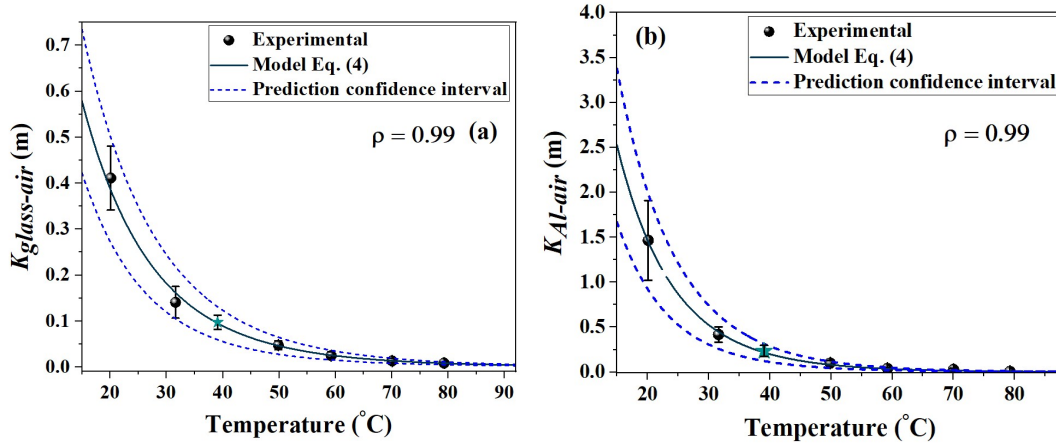
328

329 **Fig. 3** – Experimental (●,★) and predicted (—) values for $K_{glass\text{-}air}$ (a) and $K_{Al\text{-}air}$ (b) as a

330 function of equilibration temperature. The symbol (●) denotes data sets used in the parameter

331 estimation and (★) indicates the measurements used as independent validation set.

332

333 **Table 3** – Parameter estimates and their associated standard deviations obtained from the fitting

334 of Eq. (4) to the experimental values of $K_{i\text{-}air}$. Correlation of parameter estimates, Eq. (8), *Final*

335 *SEE* and *Chi²* limits for model adequacy are also summarised.

Estimates	Glass	Aluminum
A_i (m)	-3.008 ± 0.101	-2.413 ± 0.104
B_i (unitless)	-20.95 ± 1.443	-28.424 ± 1.547
Statistical analysis of estimated parameters and model adequacy		
ρ_{AB} [a]	0.27	-0.61

Final SSE	0.58	1.69
Chi² limits for adequacy [b]	0.48 < *Final SSE* < 11.14	

As it can be seen from Fig. 3, predicted values for $K_{glass\text{-}air}$ and $K_{Al\text{-}air}$ presented excellent agreement with experimental observations, with linear correlation coefficients being equal to 0.99. In addition, Fig. 3 also presents quantified averages for $K_{glass\text{-}air}$ and $K_{Al\text{-}air}$ at 40 ˚C (represented as '★') which have not been used in the parameter estimation. As it can be also seen, these measurements support the validity of the developed relationships for predicting $K_{glass\text{-}air}$ and $K_{Al\text{-}air}$ within the range of investigated temperatures. In addition, it is also important to note that although the role of RH may be important for the partition behaviour of some compounds depending on the surface sink material (Mader and Pankow, 2000; Morrison et al., 2015b; Storey et al., 1995), our results suggest that effects from the competitive adsorption between water and DEP molecules on the investigated adsorptive surfaces could be neglected within evaluated experimental ranges, as developed relationships were able to accurately predict experimental observations despite different RH conditions (Table 2).

Table 3 also presents the correlation of parameter estimates, as calculated using Eq. (8), demonstrating how the reparameterisation of the integrated form of the van't Hoff equation with the selected reference temperature was efficient in reducing the characteristic high correlation observed for parameter estimates from Arrhenius-like functions, thus improving the quality of the parameter estimation procedure (Schwaab and Pinto, 2007a). Fig. S6 illustrates the confidence region of parameter estimates as calculated using Eq. (10), where the broad shape of the regions further illustrates the low correlation between the A_i and B_i estimated coefficients. Finally, model adequacy was also confirmed by the comparison of the objective

358 function at the point of minimum (*Final SSE*) with the limits of the Chi^2 distribution with 4

359 degrees of freedom and a 95% confidence level, as illustrated in Table 3.

360   Table 4 summarises the calculated values for the pre-exponential factors of the

361 integrated form of the van't Hoff equation ($K_{glass-air,T_{ref}}$ and $K_{Al-air,T_{ref}}$), which represents the

362 value of $K_{glass-air}$ and K_{Al-air} at the reference temperature, and the values obtained for the DEP

363 adsorption/desorption enthalpy, $\Delta H°$. For $K_{i-air,T_{ref}}$, similar values to the experimentally

364 observed ones have been verified (see Table 2 and 3), as expected. In turn, calculated

365 enthalpies, equal to -56.1 ± 3.86 and -76.1 ± 4.14 kJ·mol^{-1} for the glass and aluminum surfaces,

366 respectively, are slightly smaller (in absolute terms) than reported values for the condensation

367 enthalpy of DEP at 298 K, equal to -82.1 ± 1.6 kJ·mol^{-1} (Gobble et al., 2014; Roháč et al.,

368 2004). This is in contrast to previous findings, in which researchers found higher enthalpies for

369 evaporation of phthalates (DEHP, DINP and DnBP) from vinyl flooring than from the pure

370 compound (Liang and Xu, 2014b). Liang and Xu concluded that there were stronger

371 interactions between the studied phthalates and vinyl flooring than within the pure

372 phthalates. Our results suggest that the opposite is true for glass and aluminium.

373

374 **Table 4** – Resultant constants calculated using Eq. (5-6) with the estimated parameters (A_i and

375 B_i) as presented in Table 3.

Calculated constants	Glass	Aluminum
$K_{i-air,T_{ref}}$ (m) [a]	$4.94 \cdot 10^{-2} \pm 5.22 \cdot 10^{-3}$	$8.96 \cdot 10^{-2} \pm 9.85 \cdot 10^{-3}$
$\Delta H°$ (kJ · mol^{-1}) [b]	-56.09 ± 3.864	-76.09 ± 4.142

376 [a] $K_{i-air,T_{ref}}$ was calculated using Eq. (5) with the estimated value of A_i (Table 3). [b]$\Delta H°$ was

377 calculated using Eq. (6) with the estimated value of B_i (Table 3) and T_{ref} defined as equal to

378 322 K for both the glass and aluminum surfaces.

379

To the best of our knowledge, this is the first work reporting the partitioning behaviour of DEP on glass and aluminum surfaces. In spite of that, some interesting comparisons can be made with previous reports. For instance, (Ghislain et al., 2017) proposed that the partition coefficient of DEHP on borosilicate glass at 23 ˚C could be predicted by Eq. (12).

$$Log\left(K_{glass}\right) = -0.51\cdot\log\left(p^*\right) - 2.88 \tag{12}$$

Although the characterisation of prediction errors was not reported, one could calculate the partition coefficient of DEHP on glass as equal to *0.33 m* by using the above relationship, assuming DEHP partial pressure as equal to $2.039 \cdot 10^{-5}$ Pa (Gobble et al., 2014). In another study, the partition coefficient of DEHP on polished glass at 25 ˚C was reported as equal to 600 *m*. At 23 ˚C, our proposed model predicts the partition coefficient of DEP between glass and air as equal to *0.31 ± 0.06 m*, being therefore likely smaller than predicted values for DEHP, as would be expected given the higher volatility of DEP. Furthermore, (Liang and Xu, 2014a) have investigated the partition behaviour of several phthalates, including DINP, DEHP, BBP and DnBP, between stainless steel and air at 25 ˚C, proposing that their partition coefficient, K_s, could be related to these compounds' vapour pressures through Eq. (13).

$$Log\left(K_s\right) = -0.53\cdot\log\left(p^*\right) + 0.63 \tag{13}$$

Using this proposed relationship, one could calculate K_s as equal to *1113.5 m* for DEHP, a value very similar to ones reported by (Wu et al., 2017) for this same phthalate and adsorptive surface. However, for an aluminum surface, the DEHP partition coefficient has been reported to be nearly reduced by half when compared to stainless steel (Wu et al., 2017). While it is unclear if Eq. (13) could be valid for DEP, one could calculate its K_s as equal to 14.55 *m* at 25 ˚C, which, if reduced by half to account for an aluminum surface, would not be so far from values estimated in our study, which ranged from approximately 1 to 2 *m* at 20 ˚C. Therefore,

403 while comparisons may be difficult, our values are in reasonable agreement with previous

404 reports.

405   Further studies are required to assess the impact of additional environmental conditions

406 on the diethyl phthalate partitioning behaviour, for instance, including ventilated (and

407 unsealed) scenarios. However, we note that sealed environments are commonly used as a

408 method of storage in museums collections and archives, where minimising the extent to which

409 an artefact perceive external fluctuations in temperature and relative humidity is a common

410 aim.

411 **4. Conclusions**

412   This work has investigated the partitioning behaviour of diethyl phthalate on

413 borosilicate glass and aluminum surfaces in a wide range of temperatures between 20 and 80 ˚C

414 for the first time. Measured partition coefficients for the glass and aluminum surfaces ranged

415 between $0.41 \pm 6.9 \cdot 10^{-3}$ and $8.48 \cdot 10^{-3} \pm 2 \cdot 10^{-3}$ m and between 1.47 ± 0.44 and $7.1 \cdot 10^{-3} \pm$

416 $1.4 \cdot 10^{-3}$ m, respectively, within the investigated temperature range.

417   In addition, it was demonstrated that the relationship between DEP partition

418 coefficients, $K_{glass\text{-}air}$, and temperature can be accurately predicted by a reparameterised form

419 of the van't Hoff equation, in which $K_{glass\text{-}air}$ values are exponentially reduced with temperature,

420 supporting the assumption that DEP adsorption enthalpy can be considered constant for the

421 investigated systems.

422   We anticipate that the developed models can prove useful for the mathematical

423 description of degradation phenomena involving plasticiser loss in modern and contemporary

424 artefacts, and also be a starting point for characterising the partitioning behaviour of this

425 historically significant phthalate on different storage materials used in museum collections and

426 archives. In addition, we hope this work will further contribute to ongoing efforts dedicated to

427 determine levels of human exposure to this and additional phthalates.

428

5. Acknowledgments

434

6. References

Afshari, A., Lundgren, B., Ekberg, L.E., 2003. Comparison of three small chamber test methods for the measurement of VOC emission rates from paint. Indoor Air 13, 156–165. https://doi.org/10.1034/j.1600-0668.2003.00146.x

Beale, E.M.L., 1960. Confidence regions in non-linear estimation. J. R. Stat. Soc. Ser. B 22, 41–88.

Bi, C., Liang, Y., Xu, Y., 2015. Fate and transport of phthalates in indoor environments and the influence of temperature: A case study in a test house. Environ. Sci. Technol. 49, 9674–9681. https://doi.org/10.1021/acs.est.5b02787

Box, G.P., Hunter, J.S., Hunter, W.G., 2005. Statistics for experimenters - Design, innovation, and discovery, Second. ed. Wiley-Interscience, John Wiley & Sons, Inc., New Jersey. https://doi.org/10.1017/S1742170510000062

Cao, J., Weschler, C.J., Luo, J., Zhang, Y., 2016. Cm-History method, a novel approach to simultaneously measure source and sink parameters important for estimating indoor exposures to phthalates. Environ. Sci. Technol. 50, 825–834. https://doi.org/10.1021/acs.est.5b04404

Clausen, P.A., Hansen, V., Gunnarsen, L., Afshari, A., Wolkoff, P., 2004. Emission of di-2-

452   ethylhexyl phithalate from PVC flooring into air and uptake in dust: Emission and

453   sorption experiments in FLEC and CLIMPAQ. Environ. Sci. Technol. 38, 2531–2537.

454   https://doi.org/10.1021/es0347944

455   Clausen, P.A., Spaan, S., Brouwer, D.H., Marquart, H., Le Feber, M., Engel, R., Geerts, L.,

456   Jensen, K.A., Kofoed-Sørensen, V., Hansen, B., De Brouwere, K., 2016. Experimental

457   estimation of migration and transfer of organic substances from consumer articles to

458   cotton wipes: Evaluation of underlying mechanisms. J. Expo. Sci. Environ. Epidemiol.

459   26, 104–112. https://doi.org/10.1038/jes.2015.35

460   Cousins, I., Mackay, D., 2000. Correlating the physical-chemical properties of phthalate

461   esters using the "three solubility" approach. Chemosphere 41, 1389–1399.

462   https://doi.org/10.1016/S0045-6535(00)00005-9

463   Da Ros, S., Aliev, A.E., del Gaudio, I., King, R., Pokorska, A., Kearney, M., Curran, K.,

464   2021. Characterising plasticised cellulose acetate-based historic artefacts by NMR

465   spectroscopy: A new approach for quantifying the degree of substitution and diethyl

466   phthalate contents. Polym. Degrad. Stab. 183, 109420.

467   https://doi.org/10.1016/j.polymdegradstab.2020.109420

468   Da Ros, S., Jones, M.D., Mattia, D., Schwaab, M., Barbosa-Coutinho, E., Rabelo-Neto, R.C.,

469   Noronha, F.B., Pinto, J.C., 2017a. Microkinetic analysis of ethanol to 1,3-butadiene

470   reactions over MgO-SiO2 catalysts based on characterization of experimental

471   fluctuations. Chem. Eng. J. 308, 988–1000. https://doi.org/10.1016/j.cej.2016.09.135

472   Da Ros, S., Schwaab, M., Pinto, J.C., 2017b. Parameter estimation and Statistical Methods.

473   Chem. Mol. Sci. Chem. Eng. 1–7. https://doi.org/10.1016/B978-0-12-409547-2.13918-

474   6

475   Eftekhari, A., Morrison, G.C., 2018. A high throughput method for measuring cloth-air

476   equilibrium distribution ratios for SVOCs present in indoor environments. Talanta 183,

250–257. https://doi.org/10.1016/j.talanta.2018.02.061

Eichler, C.M.A., Wu, Y., Cao, J., Shi, S., Little, J.C., 2018. Equilibrium relationship between SVOCs in PVC products and the air in contact with the product. Environ. Sci. Technol. 52, 2918–2925. https://doi.org/10.1021/acs.est.7b06253

Ellington, J.J., Floyd, T.L., 1996. Octanol/water partition coefficients for eight phthalates esters. Unites States Environmental Protection Agency: Environmental Research Brief No EPA/600/S-96/006.

Even, M., Hutzler, C., Wilke, O., Luch, A., 2020. Emissions of volatile organic compounds from polymer-based consumer products: Comparison of three emission chamber sizes. Indoor Air 30, 40–48. https://doi.org/10.1111/ina.12605

Finizio, A., Mackay, D., Bidleman, T., Harner, T., 1997. Octanol-air partition coefficient as a predictor of partitioning of semi-volatile organic chemicals to aerosols. Atmos. Environ. 31, 2289–2296.

Fromme, H., Lahrz, T., Piloty, M., Gebhart, H., Oddoy, A., Ruden, H., 2004. Occurrence of phthalates and musk fragrances in indoor air and dust from apartments and kindergartens in Berlin (Germany). Indoor Air 14, 188–195. https://doi.org/10.1046/j.1600-0668.2003.00223.x

Ghislain, M., Beigbeder, J., Plaisance, H., Desauziers, V., 2017. New sampling device for on-site measurement of SVOC gas-phase concentration at the emitting material surface. Anal. Bioanal. Chem. 409, 3199–3210. https://doi.org/10.1007/s00216-017-0259-0

Gobble, C., Chickos, J., Verevkin, S.P., 2014. Vapor pressures and vaporization enthalpies of a series of dialkyl phthalates by correlation gas chromatography. J. Chem. Eng. Data 59, 1353–1365. https://doi.org/10.1021/je500110d

IHS Markit, 2018. Plasticizers - Chemical Economics Handbook.

Kennedy, J., Eberhart, R., 1995. Particle Swarm Optimization, in: Proceedings of the IEEE

International Conference on Neural Networks. Perth, pp. 1942–1948.

https://doi.org/10.1109/ICNN.1995.488968

King, R., Grau-Bové, J., Curran, K., 2020. Plasticiser loss in heritage collections: its

prevalence, cause, effect, and methods for analysis. Herit. Sci. 8, 1–17.

https://doi.org/10.1186/s40494-020-00466-0

Koretsky, M.D., 2013. Engineering and chemical thermodynamics, 2nd ed. John Wiley &

Sons, Inc.

Kotowska, U., Garbowska, K., Isidorov, V.A., 2006. Distribution coefficients of phthalates

between absorption fiber and water and its using in quantitative analysis. Anal. Chim.

Acta 560, 110–117. https://doi.org/10.1016/j.aca.2005.12.022

Liang, Y., Xu, Y., 2014a. Improved method for measuring and characterizing phthalate

emissions from building materials and its application to exposure assessment. Environ.

Sci. Technol. 48, 4475–4484. https://doi.org/10.1021/es405809r

Liang, Y., Xu, Y., 2014b. Emission of phthalates and phthalate alternatives from vinyl

flooring and crib mattress covers: The influence of temperature. Environ. Sci. Technol.

48, 14228–14237. https://doi.org/10.1021/es504801x

Macht, M.L., Fletcher, D.A., 1938. Cellulose acetate molding compositions. Eur. J. Polit.

Res. Polit. Data Yearb. US2109593. https://doi.org/10.1111/2047-8852.12112

Mader, B.T., Pankow, J.F., 2000. Gas/solid partitioning of semivolatile organic compounds

(SOCs) to air filters. 1. Partitioning of polychlorinated dibenzodioxins, polychlorinated

dibenzofurans and polycyclic aromatic hydrocarbons to teflon membrane filters. Atmos.

Environ. 34, 4879–4887. https://doi.org/10.1016/S1352-2310(00)00241-7

Miles-Richardson, S.R., 2017. Public health implications of phthalates: a review of findings

from the U.S. national toxicology program's expert panel reports, in: Wypych, G. (Ed.),

Handbook of Plasticizers. ChemTec Publising, pp. 708–720.

527   Monakhova, Y.B., Kuballa, T., Leitz, J., Lachenmeier, D.W., 2011. Determination of diethyl

528   phthalate and polyhexamethylene guanidine in surrogate alcohol from Russia. Int. J.

529   Anal. Chem. 2011, 1–7. https://doi.org/10.1155/2011/704795

530   Mondal, S., Mukherjee, S., 2020. Long-term dietary administration of diethyl phthalate

531   triggers loss of insulin sensitivity in two key insulin target tissues of mice. Hum. Exp.

532   Toxicol. 39, 984–993. https://doi.org/10.1177/0960327120909526

533   Morrison, G., Li, H., Mishra, S., Buechlein, M., 2015a. Airborne phthalate partitioning to

534   cotton clothing. Atmos. Environ. 115, 149–152.

535   https://doi.org/10.1016/j.atmosenv.2015.05.051

536   Morrison, G., Shakila, N. V., Parker, K., 2015b. Accumulation of gas-phase

537   methamphetamine on clothing, toy fabrics, and skin oil. Indoor Air 25, 405–414.

538   https://doi.org/10.1111/ina.12159

539   Mossman, S., 1997. Perspectives on the History and Technology of Plastics, in: Mossman, S.

540   (Ed.), Early Plastics Perspectives 1850-1950. Leicester University Press, London, p.

541   1997.

542   Naumova, Y.Y., Offenberg, J.H., Eisenreich, S.J., Meng, Q., Polidori, A., Turpin, B.J.,

543   Weisel, C.P., Morandi, M.T., Colome, S.D., Stock, T.H., Winer, A.M., Alimokhtari, S.,

544   Kwon, J., Maberti, S., Shendell, D., Jones, J., Farrar, C., 2003. Gas/particle distribution

545   of polycyclic aromatic hydrocarbons in coupled outdoor/indoor atmospheres. Atmos.

546   Environ. 37, 703–719. https://doi.org/10.1016/S1352-2310(02)00820-8

547   Noronha, F.B., Pinto, J.C., Monteiro, J.L., Lobao, M.W., Santos, T.J., 1993. ESTIMA: Um

548   pacote computacional para estimação de parâmetros e Pprojeto de experimentos. Rio de

549   Janeiro.

550   Richardson, E., Truffa Giachet, M., Schilling, M., Learner, T., 2014. Assessing the physical

551   stability of archival cellulose acetate films by monitoring plasticizer loss. Polym.

552   Degrad. Stab. 107, 231–236. https://doi.org/10.1016/j.polymdegradstab.2013.12.001

553   Roháč, V., Růžička, K., Růžička, V., Zaitsau, D.H., Kabo, G.J., Diky, V., Aim, K., 2004.

554   Vapour pressure of diethyl phthalate. J. Chem. Thermodyn. 36, 929–937.

555   https://doi.org/10.1016/j.jct.2004.07.025

556   Saini, A., Okeme, J.O., Mark Parnis, J., McQueen, R.H., Diamond, M.L., 2017. From air to

557   clothing: characterizing the accumulation of semi-volatile organic compounds to fabrics

558   in indoor environments. Indoor Air 27, 631–641. https://doi.org/10.1111/ina.12328

559   Schripp, T., Salthammer, T., Fauck, C., Bekö, G., Weschler, C.J., 2014. Latex paint as a

560   delivery vehicle for diethylphthalate and di-n-butylphthalate: Predictable boundary layer

561   concentrations and emission rates. Sci. Total Environ. 494–495, 299–305.

562   https://doi.org/10.1016/j.scitotenv.2014.06.141

563   Schwaab, M., Biscaia, E.C., Monteiro, J.L., Pinto, J.C., 2008. Nonlinear parameter estimation

564   through particle swarm optimization. Chem. Eng. Sci. 63, 1542–1552.

565   https://doi.org/10.1016/j.ces.2007.11.024

566   Schwaab, M., Pinto, J.C., 2007a. Optimum reference temperature for reparameterization of

567   the Arrhenius equation. Part 1: Problems involving one kinetic constant. Chem. Eng.

568   Sci. 62, 2750–2764. https://doi.org/10.1016/j.ces.2008.03.010

569   Schwaab, M., Pinto, J.C., 2007b. Analise de Dados Experimentais I - Fundamentos de

570   Estatística e Estimação de Parâmetros. e-papers, Rio de Janeiro.

571   Sekizawa, J., Dobson, S., Touch, R.J., 2003. Concise international chemical assessment

572   document 52: Diethyl phythalate, IPCS. World Health Organization.

573   Shashoua, Y., 2008. Conservation of Plastics, 1st ed. Elsevier Ltd., Oxford.

574   Storey, J.M.E., Luo, W., Isabelle, L.M., Pankow, J.F., 1995. Gas/solid partitioning of

575   semivolatile organic compounds to model atmospheric solid surfaces as a function of

576   relative humidity. 1. Clean quartz. Environ. Sci. Technol. 29, 2420–2428.

577   Strlič, M., Thickett, D., Taylor, J., Cassar, M., 2013. Damage functions in heritage science.

578   Stud. Conserv. 58, 80–87. https://doi.org/10.1179/2047058412Y.0000000073

579   Vasiljevic, T., Su, K., Harner, T., 2021. A first look at atmospheric concentrations and

580   temporal trends of phthalates in distinct urban sectors of the Greater Toronto Area 12,

581   173–182. https://doi.org/10.1016/j.apr.2020.10.019

582   Walsh, J.F., Smith, H.E., Caprio, A.F., 1933. Plastic composition containing cellulose

583   derivatives. US1927143. https://doi.org/10.1145/178951.178972

584   Wei, W., Mandin, C., Ramalho, O., 2018. Influence of indoor environmental factors on mass

585   transfer parameters and concentrations of semi-volatile organic compounds.

586   Chemosphere 195, 223–235. https://doi.org/10.1016/j.chemosphere.2017.12.072

587   Wei, W., Ramalho, O., Mandin, C., 2019. A long-term dynamic model for predicting the

588   concentration of semivolatile organic compounds in indoor environments: Application

589   to phthalates. Build. Environ. 148, 11–19.

590   https://doi.org/10.1016/j.buildenv.2018.10.044

591   Weschler, C.J., Salthammer, T., Fromme, H., 2008. Partitioning of phthalates among the gas

592   phase, airborne particles and settled dust in indoor environments. Atmos. Environ. 42,

593   1449–1460. https://doi.org/10.1016/j.atmosenv.2007.11.014

594   Wu, Y., Eichler, C.M.A., Leng, W., Cox, S.S., Marr, L.C., Little, J.C., 2017. Adsorption of

595   Phthalates on Impervious Indoor Surfaces. Environ. Sci. Technol. 51, 2907–2913.

596   https://doi.org/10.1021/acs.est.6b05853

597   Wypych, G. (Ed.), 2017. Plasticizers in Various Industrial Products, in: Handbook of

598   Plasticizers. ChemTec Publishing, Toronto, pp. 495–605.

599   Xu, Y., Little, J.C., 2006. Predicting emissions of SVOCs from polymeric materials and their

600   interaction with airborne particles. Environ. Sci. Technol. 40, 456–461.

601   https://doi.org/10.1021/es051517j

602   Yang, C., Harris, S.A., Jantunen, L.M., Kvasnicka, J., Nguyen, L. V., Diamond, M.L., 2020.

603   Phthalates: Relationships between air, dust, electronic devices, and hands with

604   implications for exposure. Environ. Sci. Technol. 54, 8186–8197.

605   https://doi.org/10.1021/acs.est.0c00229

606   Yuan, H., Hao, Q., Su, R., Qi, W., He, Z., 2019. Migration of phthalates from polyvinyl

607   chloride film to fatty food simulants: experimental studies and model application. J. fur

608   Verbraucherschutz und Leb. 15, 135–143. https://doi.org/10.1007/s00003-019-01249-x

609   Zimmerli, A., 1932. Plastic composition, film, or article and process of making the same.

610   US1842640. https://doi.org/10.1145/178951.178972

611